Functionalized α-helical peptide hydrogels for neural tissue engineering

ACS Biomaterials SCIENCE & ENGINEERING

Article

pubs.acs.org/journal/abseba

Functionalized α-Helical Peptide Hydrogels for Neural Tissue Engineering

Nazia Mehrban,[†] Bangfu Zhu,[‡] Francesco Tamagnini,[§] Fraser I. Young,[‡] Alexandra Wasmuth,[†] Kieran L. Hudson,[†] Andrew R. Thomson,[†] Martin A. Birchall,[⊥] Andrew D. Randall,[§] Bing Song,*[,‡] and Derek N. Woolfson*[,†,#,∥]

[†]School of Chemistry, University of Bristol, Bristol BS8 1TS, United Kingdom
[‡]School of Dentistry, Cardiff University, Cardiff CF10 3XQ, United Kingdom
[§]Medical School, University of Exeter, Exeter EX4 4PS, United Kingdom
[⊥]University College London Ear Institute, London WC1X 8DA, United Kingdom
[#]School of Biochemistry, University of Bristol, Bristol BS8 1TD, United Kingdom
[∥]BrisSynBio, University of Bristol, Bristol BS8 1TQ, United Kingdom

Supporting Information

ABSTRACT: Trauma to the central and peripheral nervous systems often lead to serious morbidity. Current surgical methods for repairing or replacing such damage have limitations. Tissue engineering offers a potential alternative. Here we show that functionalized α-helical-peptide hydrogels can be used to induce attachment, migration, proliferation and differentiation of murine embryonic neural stem cells (NSCs). Specifically, compared with undecorated gels, those functionalized with Arg-Gly-Asp-Ser (RGDS) peptides increase the proliferative activity of NSCs; promote their directional migration; induce differentiation, with increased expression of microtubule-associated protein-2, and a low expression of glial fibrillary acidic protein; and lead to the formation of larger neurospheres. Electrophysiological measurements from NSCs grown in RGDS-decorated gels indicate developmental progress toward mature neuron-like behavior. Our data indicate that these functional peptide hydrogels may go some way toward overcoming the limitations of current approaches to nerve-tissue repair.

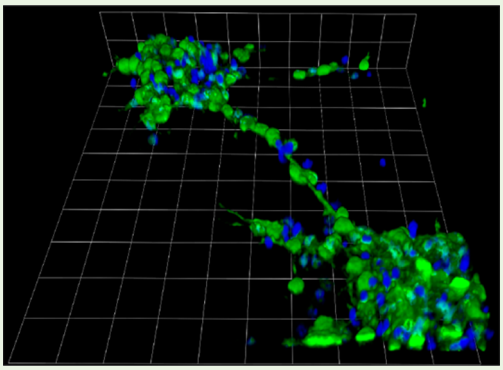

KEYWORDS: *hydrogel, nerve tissue engineering, peptide, RGD peptide, self-assembly, stem cell*

INTRODUCTION

Trauma to the central and peripheral nervous systems (CNS and PNS, respectively) can lead to severe disabilities, with injuries causing progressive degeneration and affecting long-term functionality of the tissue. In vivo repair of nervous tissue is complicated by the slow migration of macrophages at the injury site, and the consequent delay in the removal of glycoproteins in myelin, among other components, which inhibit neural tissue regeneration.[1−3] In addition, the lack of upregulation of adhesion molecules and development of glial scarring at the site of the injury culminate to create an environment hostile to functional regeneration.[4,5]

Neural tissue complexity, donor-site morbidity, and limited tissue availability in autologous tissue grafts result in loss of nerve functionality that cannot be restored using surgical methods alone; often resulting in the recruitment of surrounding nerves to compensate for the damaged tissue. Nonetheless, in the absence of functionally superior alternatives, autologous grafts remain the preferred treatment.[6,7] These limitations suggest a need for alternative methods for nerve-tissue repair.

To devise new approaches to neural-tissue repair, first we need to understand the surrounding chemical and physical niche. This is because the extracellular matrix (ECM) influences cell morphology and function.[8,9] Research in this area has significantly advanced from using allografts,[10,11] xenografts,[12−14] and decellularized tissue for neural repair to the development of bespoke tissue-engineered products that match in vivo conditions more closely.[15,16] To achieve this, both natural and synthetic materials have been used to support the proliferation and differentiation of isolated neuronal cells, including neural stem cells (NSCs). Natural scaffolds such as ECM proteins fibronectin, laminin, and collagen have been explored extensively, but with varied degrees of success;[17−20] ultimately, it has been recognized that controlling the natural material's chemical and physical properties is difficult.[21] Although synthetic materials such as poly(lactic-*co*-glycolic acid), poly(urethane), and

Received: January 30, 2015
Accepted: April 28, 2015
Published: April 28, 2015

DOI: 10.1021/acsbiomaterials.5b00051
ACS Biomater. Sci. Eng. 2015, 1, 431−439

biodegradable glass offer tighter control over many such properties,[22−26] their compatibility with basic cell functions such as growth, differentiation, and tissue formation is reduced.[21,27]

The natural progression is to combine favorable elements of both natural and synthetic systems to produce materials that allow cellular attachment, migration, proliferation and differentiation, and for the diffusion of waste and nutrients in and out of the scaffolds. To this end, a number of materials have been produced, including some based on self-assembling peptides. For example, β-sheet-based systems have been explored using NSCs with some success,[28,29] as have hybrid peptide−organic[30] and peptide−polymer systems.[31,32] Here we present the functionalization and use of hydrogelating self-assembling fibers (hSAFs).[33] This α-helical coiled-coil peptide system has been purpose-designed to mimic some of the biochemical and morphological properties of ECM. It forms porous hydrogels, which are suitable for the growth of model neural cells (Figure S1).[34]

To mimic the complexity of native ECM further, we need chemical cues to stimulate cells at different stages of tissue development: for example, fibronectin is expressed in early neuronal development to promote the growth of radial glial processes in the ventricular zone; and laminin is implicated in the migration of neurons.[35−37] Furthermore, fibronectin is maintained at low levels in the Schwann cell basement membrane of adult peripheral nerves,[38] but is rapidly upregulated following injury in both the PNS[39] and CNS,[40−43] and is recognized by at least 10 different integrin receptors on the cell surface through various combinations of α and β subunits.[44] Thus, the expression of guidance cues that stimulate and govern neuronal recruitment and differentiation, including fibronectin, are complex and highly dynamic.

Here, we focus on a cell-adhesion cue from fibronectin, namely the Arg-Gly-Asp-Ser (RGDS) sequence,[34] appending it to hSAF gels, and following its effects on primary NSC attachment, migration, proliferation, differentiation, and electrophysiology at the early stages of cell development.

MATERIALS AND METHODS

An expanded version of all the Materials and Methods used for this study is available in the Supporting Information.

Scaffold Formation. Peptides were synthesized using standard solid-phase peptide synthesis protocols on a CEM "Liberty" microwave-assisted peptide synthesizer. Peptides were purified by reversed-phase HPLC and their masses confirmed by MALDI-TOF mass spectrometry. Typically, hSAF gels were prepared by mixing separate 2 mM stock solutions for each of the complementary peptides (hSAF-p1 or hSAF-p1(N_3), plus hSAF-p2) in 20 mM MOPS (3-*N*-morpholino)-propanesulfonic acid, 5 mM sodium acetate, 1 mM EDTA) buffer at pH 7.4. This gave final solutions of 1 mM of each peptide. These were left on ice for 10 min followed by overnight incubation at 4 °C, resulting in gels. For decoration experiments hSAF-p1(N_3) was substituted for hSAF-p1. After gel formation RGDS-decoration was performed by addition of 2 mM alk-RGDS and $CuSO_4$ and ascorbic acid, each at 4 mM final concentration, at 4 °C overnight. As described previously,[34] this click reaction proceeds to ∼90%, presumably because some of the hSAF-p1(N_3) peptides are protected through fiber/gel formation. Thus, we anticipate that ∼90% of the hSAF-p1(N_3) peptide, and 45% of the hSAF scaffold in total, should be decorated with RGDS units through this procedure. Gels were then washed with 10 mM EDTA (ethylenediaminetetraacetic acid) buffer, PBS (phosphate buffered saline), and NSC media. Half-moon gels were formed in 24-well cell-culture plates using sterile glass coverslips as temporary separators for the undecorated hSAF and RGDS-decorated hSAF gels (Figure S1).[34] Decoration of the hSAF-p1(N_3) half of the gel was achieved as outlined above. Laminin scaffolds were formed by coating the tissue-culture plates with poly-D-lysine for 1 h, washing with PBS and incubating with laminin solution at 37 °C for 30 min. The plates were washed with PBS before use. All gels were made to thicknesses of ∼2 mm.

Murine Embryonic Neural Stem Cell (NSC) Isolation and Culture. Meninges were isolated from embryonic E12−E14 C57/Black6 murine cortices into ice-cold DMEM/F-12 media containing penicillin−streptomcyin. After tissue digestion in accutase at 37 °C for 10 min, the isolated cells were centrifuged, resuspended in NSC media, and incubated at 37 °C, 5% CO_2. GFP-positive cells were produced according to a previously reported protocol[45] and incubated at 37 °C, 5% CO_2. Media was replaced every 3 days and the cells passaged every 6 days. After cell expansion, neurospheres were digested into single-cell suspensions using accutase and resuspended in fresh NSC media before being passed through a 40 μm cell strainer to remove remaining neurospheres. The cells were counted in the presence of Trypan Blue, seeded at a density of 0.5×10^4 in 96 wells and 1.0×10^4 in 24 wells, and incubated at 37 °C, 5% CO_2.

Cell Studies. The proliferation rate of NSCs on hSAF and laminin gels was evaluated by an MTT (3-(4,5-dimethylthiazol-2-yl)-2,5-diphenyltetrazolium bromide) metabolic activity absorbance assay (Figure S3; protocol adapted from ref 46). For assessing cell migration, time-lapse images of NSC-seeded half-moon gels were recorded every 10 min for 24 h. Migration was quantified as described previously.[47] For protein expression and fluorescence microscopy cells were fixed with paraformaldehyde, their membranes permeabilized, nonspecific binding blocked with bovine serum albumin at 22 °C for 30 min before rabbit polyclonal anti-MAP2 and mouse monoclonal anti-GFAP primary antibodies were added to the samples and left at 4 °C overnight. The samples were then washed with PBS-Triton X-100 before TRITC-conjugated (Alexa Fluor 594) goat antimouse and antirabbit secondary antibody IgG was added and left at 22 °C for 1h. After further washing steps, the samples were mounted using a DAPI (4′,6-diamidino-2-phenylindole)-containing medium and imaged on a Delta-vision microscope system using either a fluorescein isothiocyanate or tetramethylrhodamine isothiocyanate filter. Z-stacks were collated on a confocal laser scanning microscope to determine the depth of cell migration into the gel. The number of processes produced by each cell were counted using ImageJ software. Electrophysiological characteristics of the cells were determined via patch-clamp tests (Figure S5). Recordings were performed after 7 and 14 days culture on gels by continuously perfusing the gels with Hank's Balanced Salt Solution containing 130 mM NaCl, 3 mM KCl, 10 mM 4-(2-hydroxyethyl)-1-piperazineethanesulfonic acid (HEPES)-free acid, 1 mM $MgCl_2$, 2 mM $CaCl_2$, and 10 mM glucose, pH 7.3, 32 °C. Cells were visualized using infrared differential interference contrast microscopy combined with epi-fluorescence and patched using glass micropipettes filled 135 mM K-gluconate, 5 mM NaCl, 10 mM K-HEPES, 200 μM EGTA, 300 μM Na-GTP, 4 mM Mg-ATP, 13.4 mM biocytin, pH 7.3. The liquid junction potential was corrected arithmetically. Following a whole-cell-recording configuration, the pipet capacitance was neutralized and the series resistance compensated (10−80% correction). Voltage-clamp recordings were made for the quantitative evaluation of voltage-gated currents.

Statistical Analysis. Data are presented in the format "mean ± standard error of the mean (SEM)". Differences in mean values were compared within groups and significant differences were determined by ANOVA (analysis of variance) with posthoc Tukey−Kramer HSD (honestly significant difference) test. The significance level was set at $p < 0.05$. For the electrophysiology experiments specifically, the maximal conductance values and the values for half the voltage that generated half the maximal conductance for K^+ current activation were compared between groups over time with two-way ANOVA. If an overall effect of gel, time, or gel versus time was observed, a Bonferroni posthoc *t* test was performed. The same approach was applied to membrane passive properties between gels over time. The time of rise between 10 and 90% of the outward current peak (10−90 time of rise) at 14 days was compared between gels with an unpaired Student's *t* test.

DOI: 10.1021/acsbiomaterials.5b00051
ACS Biomater. Sci. Eng. 2015, 1, 431−439

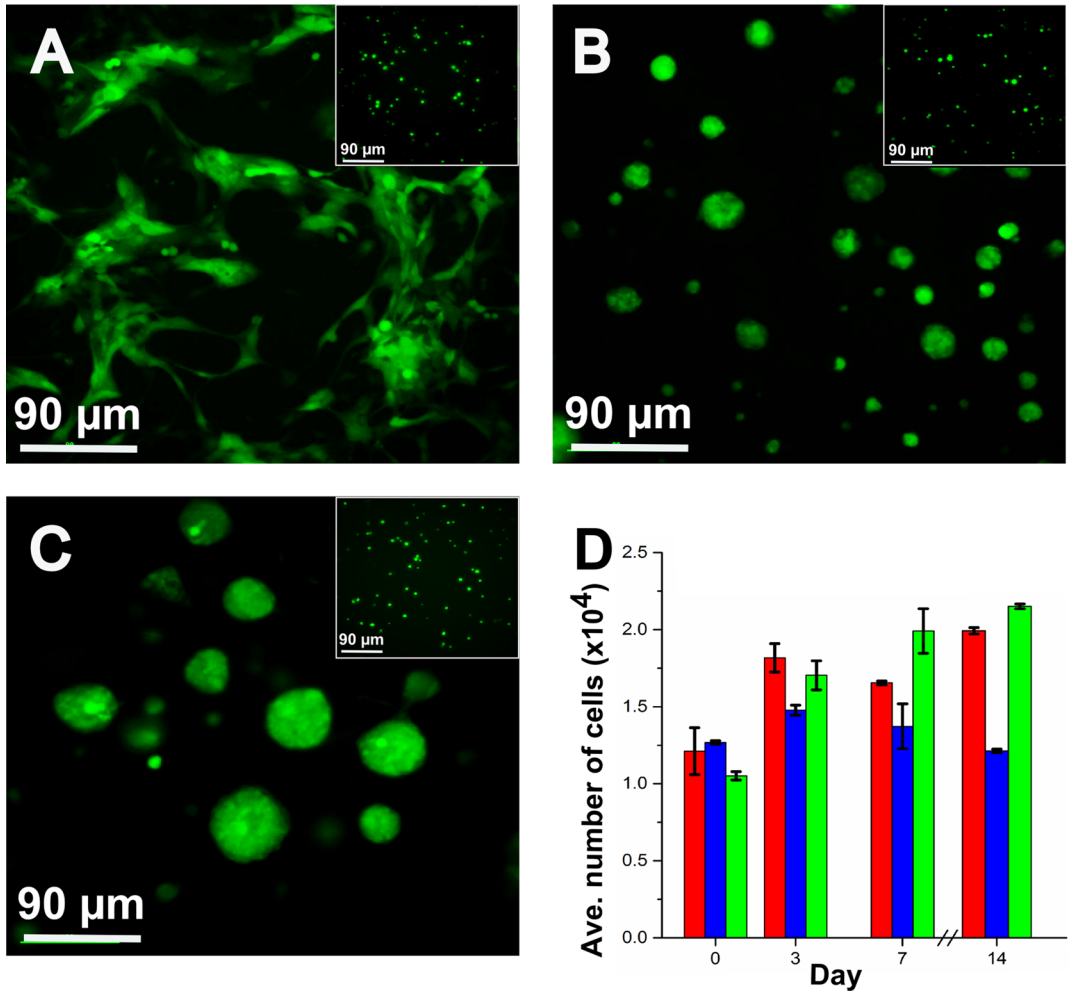

Figure 1. Nestin expression and proliferation of NSCs on hSAF and laminin gels. (A–D) Single-cell suspension of GFP-nestin positive murine NSCs (green) seeded on (A) laminin, (B) undecorated hSAF, and (C) RGDS-decorated hSAF gels. Main panels, Day 14; insets, Day 0. (A–C) Day 14. (D) Proliferative activity of NSCs on laminin (red), undecorated hSAF (blue), and RGDS-decorated hSAF (green) gels over 14 days as measured by an MTT assay (n = 3 for each time point).

RESULTS

Expression of Progenitor Characteristics, Proliferative Activity, and Formation of Neurospheres. First, we compared the response of NSCs to seeding on different substrates; specifically, undecorated and RGDS-decorated hSAF gels with laminin gels as a control (Figure 1). We followed this using GFP-labeled nestin. This showed that NSCs expressed the predifferentiation, intermediate-filament-protein marker[48] on all three substrates over 14 days (Figure 1A–C and Figure S2), and therefore retained their ability to differentiate into specific lineages. In addition, a standard MTT metabolic assay showed that, although the majority of NSCs on the undecorated hSAF gels survived the course of the study, the proliferative activity remained the same over this period (Figure 1D). By contrast, on the RGDS-decorated gels, this activity doubled over the two-week time course, mirroring that seen for cells seeded on control laminin gels (Figure 1D). Finally, the appearances of the cells on the three substrates were very different over time: by day 14, those seeded on laminin were more spread out (Figure 1A); whereas, those on the hSAFs were clumped together (we refer to these as "neurospheres"). Moreover, the neurospheres formed on the decorated hSAFs were much larger than those observed on the undecorated gels (Figure 1B, C).

Further analysis of the neurospheres showed that the cells extended in the X-, Y-, and Z-directions creating 3D clusters embedded within the hSAF gels, compared with relatively flat cultured cells on the laminin substrate (Figure 2A–C, Videos S1–S3). For the former, the sizes of the neurospheres varied considerably between gel types with the cell layer on RGDS-decorated gels being much thicker than those on undecorated gels (36 ± 8 μm and 20 ± 2 μm, respectively), which were both thicker than with the laminin substrate (9 ± 1 μm). Cells on RGDS-decorated gels also formed connections between the neurospheres (Figure 2D, Video S4), which were less apparent on the undecorated gels.

Directional Migration of Cells. We found that even without added growth factors, the RGDS functionality promoted NSC migration. To follow this, we used time-lapse images and spider-plot analysis of cell migration on laminin as a controls, and "half-moon gels" in which undecorated and RGDS-decorated hSAFs were prepared side-by-side in the same cell-culture well[34] (Figure 3A–H). These revealed random migration of cells from their starting positions on all three gels (Figure 3I–K, Videos S5–S7). However, analysis of the border of the undecorated and RGDS-decorated hSAF gels in the half-moon experiments clearly indicated preferential migration of NSCs toward the decorated side (Figure 3H, L, Video S8). There was little difference in the

DOI: 10.1021/acsbiomaterials.5b00051
ACS Biomater. Sci. Eng. 2015, 1, 431–439

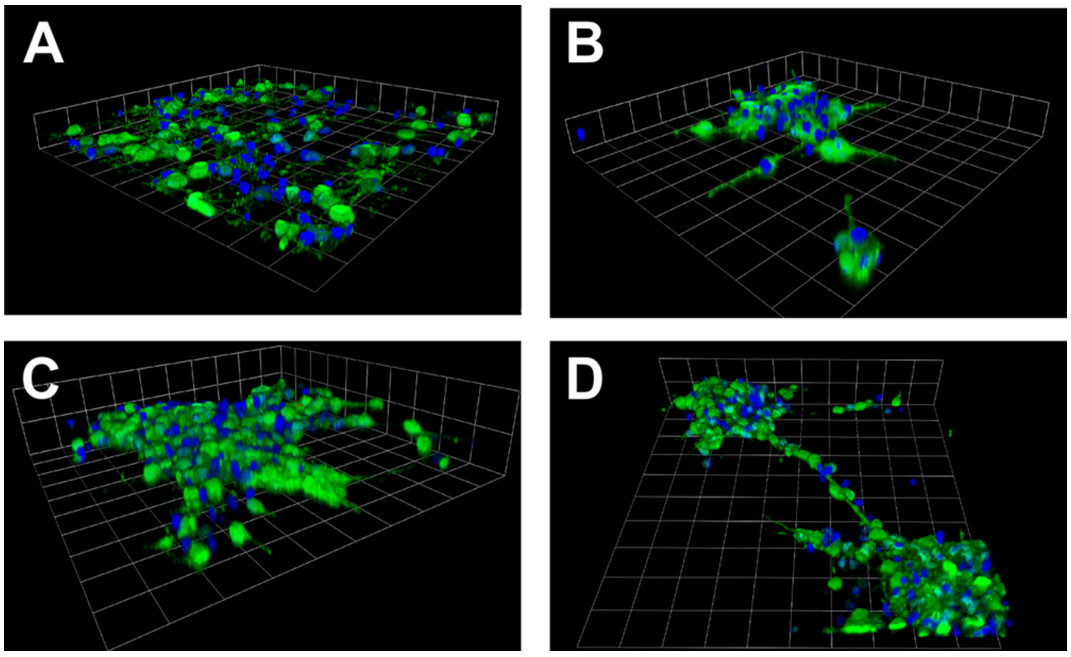

Figure 2. 3D neurosphere formation by NSCs in hSAF gels. 3D reconstruction of z-stack fluorescent images on (A) laminin, (B) undecorated hSAF, and (C) RGDS-decorated hSAF gels. (D) 3D reconstruction of z-stack fluorescent images of cells on RGDS-decorated gels showing neurosphere connections. DAPI-stained cell nuclei (blue) and nestin expression (green). (A–D) Grid scales: 24.75 μm.

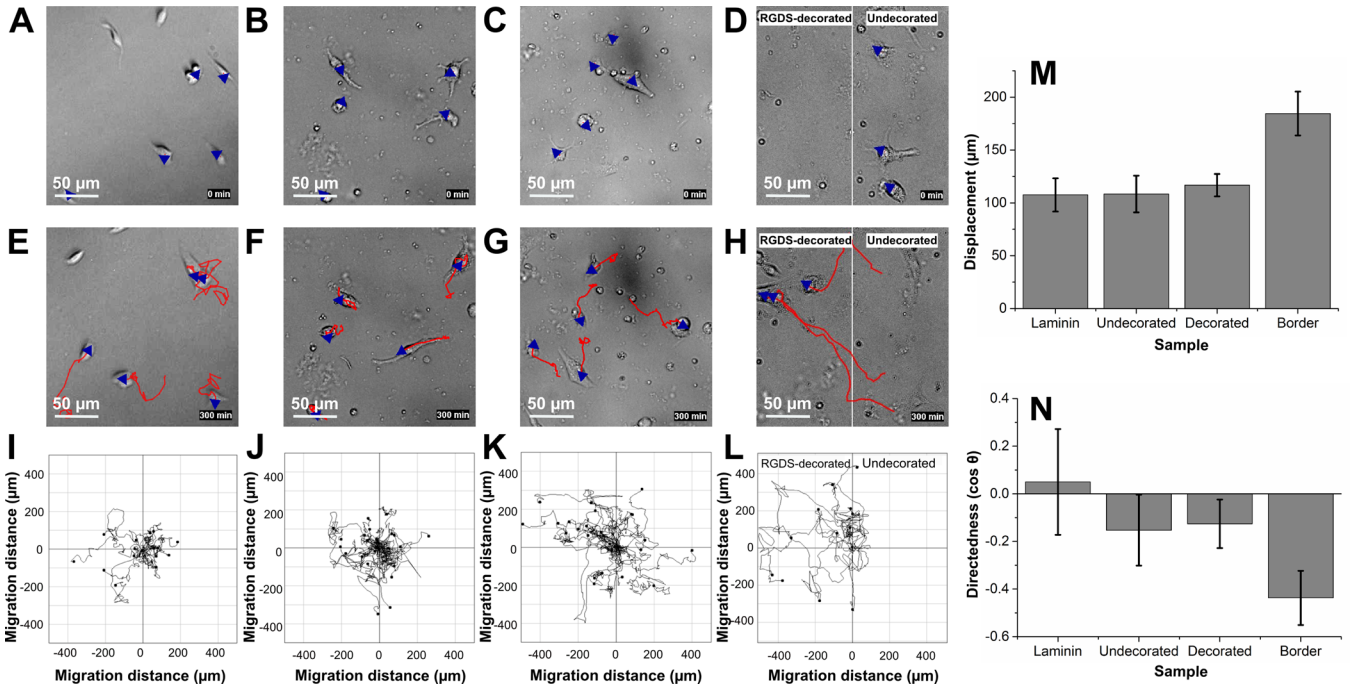

Figure 3. Migration of NSCs across half-moon hSAF, and laminin gels. (A–H) First and last frames of NSC migration captured over 24 h. (A) Bright-field images of NSCs on laminin, (B) undecorated hSAF, (C) RGDS-decorated hSAF gels, and (D) the border between an undecorated and RGDS-decorated hSAF half-moon gel. Blue arrowheads indicate the direction of cell migration. (E–H) Final frame bright-field images of NSCs on (E) laminin, (F) undecorated hSAF, (G) RGDS-decorated hSAF gels, and (H) the border between an undecorated and RGDS-decorated hSAF half-moon gel at 24 h postseeding. Migration tracks (red) indicate the overall movement over this period; and the arrowheads indicate direction of cell migration. (I–K) Migration tracks of cells over 24 h on (I) laminin, (J) undecorated hSAF, (K) RGDS-decorated hSAF gels, and (L) the border between an undecorated and RGDS-decorated hSAF half-moon gel represented as spider plots. Each line indicates a separate cell showing the start (center of the plot) and end (black dot) positions of each cell. (M) Displacement of cells over 24 h. (N) Directedness of cells over 24 h: migration in the y-direction ($\cos\theta = 0$), to the right ($\cos\theta = +1$), and to the left ($\cos\theta = -1$) are presented. n = 15 (laminin), 24 (undecorated hSAF), 48 (RGDS-decorated hSAF), and 12 (border between undecorated and RGDS-decorated gels).

displacement and directionality of the cells on laminin, and on distinct regions of the undecorated, RGDS-decorated hSAFs, (Figure 3M, N, first three bars). However, when presented with the border of the two different hSAF chemistries, cells migrated

DOI: 10.1021/acsbiomaterials.5b00051
ACS Biomater. Sci. Eng. 2015, 1, 431–439

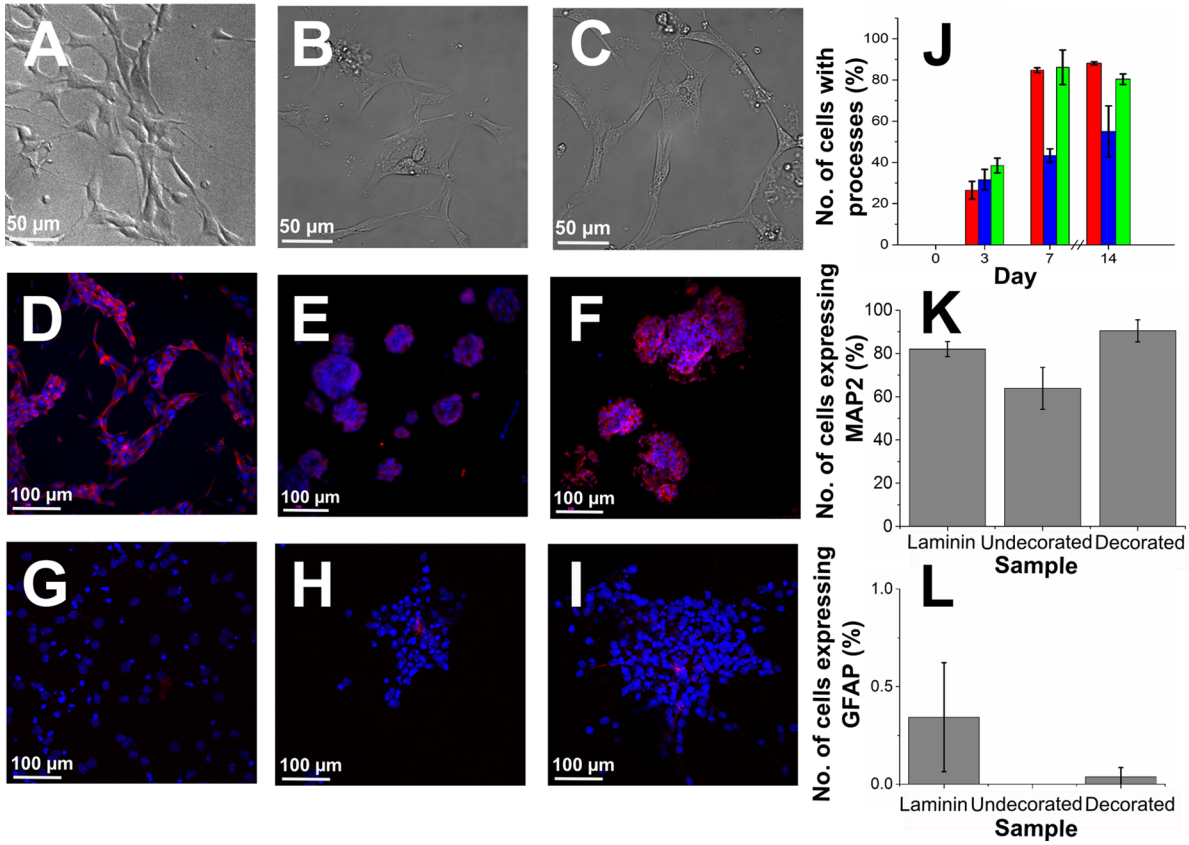

Figure 4. Differentiation of NSCs on hSAF and laminin gels. (A, D, G) laminin; (B, E, F) undecorated hSAF; (C, F, I) RGDS-decorated hSAF gels. (A–C) Phase-contrast images showing cell morphology at day 7. (D–F) Representative fluorescent images show NSC expression of MAP2 (red) and DAPI-stained nuclei (blue) on all gels. (G–I) Representative fluorescent images show NSC expression of GFAP (red) and DAPI-stained nuclei (blue) on all gels. (J) Percentage of cells producing processes after 14 days in culture on laminin (red), undecorated hSAF (blue) and RGDS-decorated hSAF (green) gels. Percentage of cells expressing the neuronal differentiation markers (K) MAP2 and (L) GFAP. $n = 3$ for all experiments.

toward the RGDS-modified side and traveled further (Figure 3M, N, fourth bars). The cells at the border also appeared to travel faster toward that side (Figure S4).

Stem Cell Differentiation. Cells seeded on all three gels produced neurite-like processes by day 7 (Figure 4A–C). This indicated that the NSCs were adhering and differentiating with an elongated cell morphology in all cases. The undecorated gels showed the lowest percentage of cells with processes, whereas those on RGDS-decorated and laminin gave similar levels (Figure 4J). Immunocytochemistry staining for microtubule-associated protein-2 (MAP2), a neural lineage specific marker, revealed it to be expressed by cells on all three gel types (Figure 4D–F). The number of cells expressing MAP2 was lowest for the undecorated hSAF gel, with cells seeded on laminin and RGDS-decorated hSAF gels showing similar levels of expression (Figure 4K). By contrast, very little glial fibrillary acidic protein (GFAP), which is associated with astrocytes or star-shaped glial cells, was expressed on any of the gels (Figure 4G–I, L).

Cell Maturation and Electrophysiological Properties. Patch-clamp recordings in voltage-clamp mode were used to evaluate the K^+ currents in NSCs cultured in undecorated and RGDS-decorated hSAF gels. Starting from a holding potential of −90 mV, 30 ms step depolarizations were applied, incrementally increasing from −80 to +30 mV. When sufficiently large depolarizations were used, clear outward K^+ currents were observed in all cells. After 7 days of culture on either substrate, these outward currents were relatively slowly activating, essentially noninactivating, reflecting an immature phenotype (Figure 5A). By day 14, however, the outward current waveform had matured in both cases, developing clearly observable degrees of current inactivation and faster rates of activation (Figure 5B). Furthermore, by this time, the contribution of the inactivating current component was significantly larger in the RGDS-decorated gel ($p < 0.001$). This was seen in the inactivating component of current, which was larger than the noninactivating current remaining at the end of the 30 ms depolarizing stimulus. In contrast, the inactivating current component amounted to only around 25% of the noninactivating current in the undecorated gel. In line with a more-mature K^+-channel complement in the RGDS-decorated hSAF gels at 14 days, the rate of current rise was faster in cells recorded on this substrate.

Analysis of the peak amplitude of the outward current across a range of test potentials from −80 to +30 mV was used to determine the conductance activated at each voltage. This was then normalized to cell capacitance, an electrical parameter directly proportional to cell-surface area, yielding specific conductance versus voltage curves. At 7 days these curves were quite similar in both gels and did not exceed 2.5 nS/pF (Figure 5C); the peak specific conductance was smaller for cells on the RGDS-decorated gel than the undecorated gel. At 14 days, however, the conductance density was clearly larger for the RGDS-decorated gel samples (Figure 5D). For these, the current density grew almost 4-fold between day 7 and 14, whereas, there was only a marginal and nonsignificant increase for the undecorated gels.

DOI: 10.1021/acsbiomaterials.5b00051
ACS Biomater. Sci. Eng. 2015, 1, 431–439

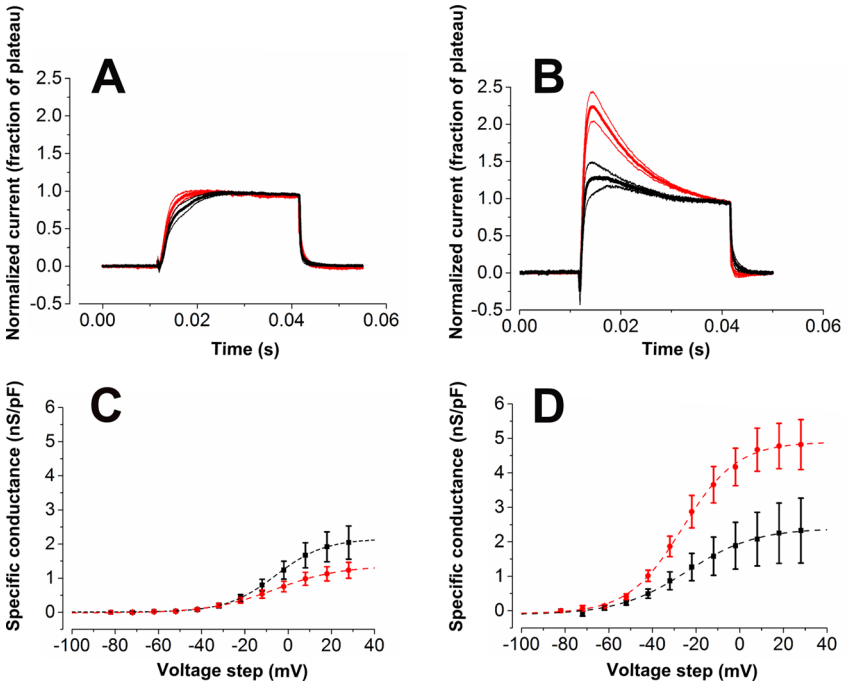

Figure 5. Activation dynamics of NSC K^+ currents on RGDS-decorated and undecorated hSAF gels at (A, C) 7 and (B, D) 14 days. (A, B) Outward K^+ currents evoked by a +80 mV voltage step, normalized to the plateau and averaged on undecorated hSAF (black) and RGDS-decorated hSAF gel (red). (C, D) Analysis of the specific conductance recorded on undecorated hSAF (black) and RGDS-decorated hSAF gel (red) with different voltage step intensities. The Boltzmann sigmoidal fit of the conductance-voltage curves at each time-point and for each gel is shown. The extrapolated maximal conductance and relative values for half the voltage that generates half the maximal conductance are reported. n = 12 (undecorated hSAF) and 14 (RGDS-decorated hSAF) for day 7 and 5 (undecorated hSAF) and 10 (RGDS-decorated hSAF) for day 14.

DISCUSSION

We have shown that it is possible to increase the attachment of murine NSCs to de novo designed peptide hydrogels (hSAFs) through the addition of a cell-adhesion motif, RGDS. This motif also influences the proliferation and differentiation rates of NSCs over 14 days. Cells produced processes and expressed MAP2, with little GFAP. Analysis of the migratory behavior of the cells indicated that, when given the option of undecorated and RGDS-decorated hSAF gels, NSCs preferentially migrated toward the RGDS-rich regions. RGDS decoration also influenced the functional electrophysiological properties. Although the cells did not fire action potentials, the RGDS-decoration promoted changes associated with mature neurons.

Furthermore, we have shown that the proliferation of NSCs led to the formation of neurospheres extending into hSAF gels, with the largest neurospheres forming in the RGDS-decorated gels. It is unlikely that the hSAF fibers are physically constricting the cells as observations made in the first day of cell culture showed cells freely migrating through the gels. Furthermore, cells formed connections between neurospheres in RGDS-decorated gels, indicating free migration. It may be that cell−cell interactions encourage neurosphere formation in hSAF gels, or vice versa. It has been shown that neural precursor cells grown as neurospheres mainly express receptors that interact with fibronectin and vitronectin.[49] Consistent with this, we did not observe neurospheres with laminin as the substrate; although we did observe these with both hSAF gel types. Such neurosphere formation may be more favorable for in vivo studies, where a small wound site would require high cell proliferative activity in order to provide a suitable environment for new tissue ingress.

Further analysis of the predifferentiation migratory behavior of the cells showed that when presented with both undecorated and RGDS-decorated hSAF chemistries the cells actively migrated toward the RGDS-decorated gels, and traveled further and faster in the zone between the two gel types. Although RGDS is primarily an adhesion sequence, in vivo studies have shown a higher expression of fibronectin in brain tissue when neurons migrate toward the cortical plate region.[36,50] Cell surface receptors bind to the RGDS sequences through focal adhesions.[51] This attachment at the leading edge of the cells encourages preferential movement toward RGDS-rich regions.[52] Movement along traction points initiated by the focal adhesions creates tension in the cell body and allows the cell to release any weaker attachments at the rear, and effect propulsion toward the RGDS side.[53] This is a repeating process of cytoskeletal reorganization, attachment, maturation and then disassembly via actomyosin contraction and so the cell is able to migrate along the surface.[54,55] We posit that this mechanism may be in play in our system. Furthermore, others show that at low adhesivity cells lack the traction needed to propel forward, while at high adhesivity the cells cannot rupture the bonds at their rear and therefore do not propel forward.[56] We suggest further that the undecorated and RGDS-decorated hSAF gels are analogous to these low and high adhesivity regions, respectively. In turn, this could explain why cells at the border between the two gel chemistries move the furthest and fastest; that is compared with those in the separated undecorated or RGDS-decorated zones, which behave more sluggishly and similarly.

Ultimately, isolating which RGDS-integrin combination is active at various stages in our system is not straightforward, and would likely require an analysis of all possible combinations of integrin α and β subunits at the adhesome, i.e., the protein−protein interaction network at the integrin-ECM level.[57] Furthermore, the "inside-out" signals governing the cell

DOI: 10.1021/acsbiomaterials.5b00051
ACS Biomater. Sci. Eng. 2015, 1, 431−439

interactions with the ECM[53] as well as the "outside-in" signals affecting the intracellular processes[58] are complex and not easily interpreted, especially in the predifferentiation stage as the cells move. For example, we recognize that laminin is a key component of extracellular matrix with many different isoforms[59,60] and that these also influence neural-cell attachment, differentiation and growth.[61] Similarly, physical and rheological differences may exist between laminin and hSAFs, which could influence cellular behavior. Nonetheless, the ability to recruit migratory neural cells as well as promoting cell attachment which we have demonstrated, allows a high level of control that may be of use in directing cells toward wound sites where the wound bed would otherwise be unfavorable for cell growth and tissue repair.[62]

For postattachment cells, we found the expression of MAP2 to be similar on RGDS-decorated hSAF and laminin gels. In vivo, MAP2 is expressed to stabilize microtubules before dendrite production and axonal maturity.[63,64] Combined, these points suggest that cells on these gels are differentiating and may be approaching maturation. However, NSC progenitor cells also have the ability to differentiate into radial glia, astrocytes and oligodendrocytes.[65] Our studies show that very little GFAP was expressed by cells on any of the gels tested. GFAP expression in particular would indicate the presence of reactive astrocytes (a major component of glial scars), which are responsible for astrogliosis; that is, the synthesis of a supportive network to fill the damaged tissue void and ultimately form a glial scar. Astrogliosis is also known to be one of the main reasons for neural, particularly axonal, regeneration failure.[66] Therefore, the lack of GFAP in our systems indicates that the regenerative capabilities of NSCs in hSAFs are being retained.

Electrophysiological experiments allowed us to further investigate how neuron-like these cells were. Neurophysiological changes are expected as the NSCs differentiate, and are influenced by many factors.[67−70] To the best of our knowledge, no such data has been recorded from de novo-designed gels. Whole-cell patch-clamp recordings showed large voltage-gated K^+ currents; ion channels that play a key role in shaping neural activity in vivo,[71] on hSAF gels. The K^+ current was highest on RGDS-decorated gels over 14 days and together with a negative shift in the voltage dependence of activation and depolarizations that exhibited a rapidly inactivating current component. The data indicate that cells on these gels are developing into mature neurons.[72−74]

CONCLUSION

In summary, we have described how functionalized peptide hydrogels (RGDS-functionalized hSAFs) can be combined with neural stem cells (NSCs) to alter and control cellular attachment and differentiation compared with unfuctionalized, control gels. Moreover, cells in competitive studies, migrate toward RGDS-rich regions of the gels. Controlling these behaviors will be crucial in recruiting cells to the wound site in vivo.

In addition, with the RGDS-functionalized hSAFs, cells form large neurospheres on the peptide gels, and show signs of maturation toward neurons. We recognize that to promote further maturation, and to mimic the complexity and continually changing environment of native neural tissue, other functionalities will have to be introduced into our system. Nonetheless, both of these responses, together with the altered cellular behaviors, are encouraging for using RGDS-functionalized hSAF gels as a starting platform for neural-tissue development and engineering.

ASSOCIATED CONTENT

Supporting Information

The Supporting Information is available free of charge on the ACS Publications website at DOI: 10.1021/acsbiomaterials.5b00051.

Figures S1−S5, descriptions of Videos S1−S8, and extended Materials and Methods (PDF)

Video S1: Depth of NSC penetration into laminin gel (AVI)

Video S2: Neurosphere formation and depth of NSC penetration into undecorated hSAF gel (AVI)

Video S3: Neurosphere formation and depth of NSC penetration into RGDS-decorated hSAF gel (AVI)

Video S4: Formation of connections between neurospheres in RGDS-decorated hSAF gel (AVI)

Video S5: Migration and spider plots of NSCs over laminin (AVI)

Video S6: Migration and spider plots of NSCs over undecorated hSAF gel (AVI)

Video S7: Migration and spider plots of NSCs over RGDS-decorated hSAF gel (AVI)

Video S8: Migration and spider plots of NSCs across the hSAF half-moon border (AVI)

AUTHOR INFORMATION

Corresponding Authors

*E-mail: D.N.Woolfson@bristol.ac.uk. Fax: +44 (0)117 929 8611).

*E-mail: SongB3@cardiff.ac.uk.

Author Contributions

N.M., B.S., and D.N.W. conceived the project. N.M., B.Z., F.T., A.D.R., B.S., and D.N.W. designed the various experiments. N.M., A.W., K.L.H., and A.R.T. made the peptides. N.M., B.Z., and F.I.Y. conducted the cell-culture experiments. NM and FT conducted the electrophysiology experiments. M.A.B., A.D.R., B.S., and D.N.W. supervised the work and raised grant support. N.M., B.Z., F.T., F.I.Y., A.D.R., B.S., and D.N.W. wrote the paper.

Funding

This work was supported by the Biotechnology and Biological Sciences Research Council (H01716X, D.N.W. and M.A.B.); the European Research Council (StG243261, BS; and ADG340764, D.N.W.); the Royal Society (UF051616, B.S.); the Medical Research Council (G1100623, A.D.R.); and the Engineering and Physical Sciences Research Council (Bristol Chemical Synthesis Centre for Doctoral Training, EP/G036764/1, K.L.H.). D.N.W. holds a Royal Society Wolfson Research Merit Award.

Notes

The authors declare no competing financial interest.

ACKNOWLEDGMENTS

We thank the D.N.W. and B.S. groups and Joe Beesley in particular for useful discussions. We are grateful to the Chemistry Electron Microscopy Unit and the Wolfson Bioimaging Facility at the University of Bristol for access to microscopes and advice. We thank Dr. Wei Cui from Imperial College London for the nestin enhancer EGFP construct.

REFERENCES

(1) Chen, J.; Lee, H. J.; Jakovcevski, I.; Shah, R.; Bhagat, N.; Loers, G.; Liu, H.-Y.; Meiners, S.; Taschenberger, G.; Kügler, S.; Irintchev, A.; Schachner, M. The Extracellular Matrix Glycoprotein Tenascin-C is

DOI: 10.1021/acsbiomaterials.5b00051
ACS Biomater. Sci. Eng. 2015, 1, 431−439

Beneficial for Spinal Cord Regeneration. *Mol. Ther.* **2010**, *18*, 1769−1777.
(2) Wong, E. V.; David, S.; Jacob, M. H.; Jay, D. G. Inactivation of Myelin-Associated Glycoprotein Enhances Optic Nerve Regeneration. *J. Neurosci.* **2003**, *23*, 3112−3117.
(3) Avellino, A. M.; Hart, D.; Dailey, A. T.; Mac-Kinnon, M.; Ellegala, D.; Kliot, M. Differential Macrophage Responses in the Peripheral and Central Nervous System during Wallerian Degeneration of Axons. *Exp. Neurol.* **1995**, *136*, 183−198.
(4) Cregg, J. M.; DePaul, M. A.; Filous, A. R.; Lang, B. T.; Tran, A.; Silver, J. Functional Regeneration Beyond the Glial Scar. *Exp. Neurol.* **2014**, *253*, 197−207.
(5) McKeon, R. J.; Schreiber, R. C.; Rudge, J. S.; Silver, J. Reduction of Neurite Outgrowth in a Model of Glial Scarring Following CNS Injury is Correlated with the Expression of Inhibitory Molecules on Reactive Astrocytes. *J. Neurosci.* **1991**, *11*, 3398−3411.
(6) Gu, X.; Ding, F.; Yang, Y.; Liu, J. Construction of Tissue Engineered Nerve Grafts and Their Application in Peripheral Nerve Damage. *Prog. Neurobiol.* **2011**, *93*, 204−230.
(7) Zhang, Y.; Lou, H.; Zhang, Z.; Lu, Y.; Huang, X.; Yang, L.; Xu, J.; Yang, W.; Fan, X.; Du, B.; Gao, P.; Hu, G.; Jin, Y. A Nerve Graft Constructed with Xenogeneic Acellular Nerve Matrix and Autologous Adipose-Derived Mesenchymal Stem Cells. *Biomaterials* **2010**, *31*, 5312−5324.
(8) Kim, D.-H.; Provenzano, P. P.; Smith, C. L.; Levchenko, A. Matrix Nanotopography as a Regulator of Cell Function. *J. Cell Biol.* **2012**, *197*, 351−360.
(9) Bellamkonda, R.; Aebischer, P. Review: Tissue Engineering in the Nervous System. *Biotechnol. Bioeng.* **1993**, *43*, 543−554.
(10) Zhong, H.; Chen, B.; Lu, S.; Zhao, M.; Guo, Y.; Hou, S. Nerve Regeneration and Functional Recovery after a Sciatic Nerve Gap is Repaired by an Acellular Nerve Allograft made through Chemical Extraction in Canines. *J. Reconstr. Microsurg.* **2007**, *23*, 479−487.
(11) Lin, M. Y.; Manzano, G.; Gupta, R. Nerve Allografts and Conduits in Peripheral Nerve Repair. *Hand. Clin.* **2013**, *29*, 331−348.
(12) Barker, R. A.; Ratcliffe, E.; Mclaughlin, M.; Richards, A.; Dunnett, S. B. A Role for Complement in the Rejection of Porcine Ventral Mesencephalic Xenografts in a Rat Model of Parkinson's Disease. *J. Neurosci.* **2000**, *20*, 3415−3424.
(13) Lu, L.-J.; Sun, J.-B.; Liu, Z.-G.; Gong, X.; Cui, J.-L.; Sun, X.-G. Immune Responses following Mouse Peripheral Nerve Xenotransplantation in Rats. *J. Biomed. Biotechnol.* **2009**, *2009*, Article ID 412598.10.1155/2009/412598
(14) Li, W.; Jia, Z.; Zhang, S.; Lin, X.; Yang, R.; He, Q.; Ruan, D. The Cellular Immune Mechanism after Transfer of Chemically Extracted Acellular Nerve Xenografts. *PLoS One* **2013**, *8*, e68806.
(15) Wang, M.; Yu, L. Transplantation of Adipose-Derived Stem Cells Combined with Decellularized Cartilage ECM: a novel approach to nasal septum perforation repair. *Med. Hypotheses* **2014**, *82*, 781−783.
(16) Zhao, B.; Sun, X.; Li, X.; Yang, Q.; Li, Y.; Zhang, Y.; Li, B.; Ma, X. Improved Preparation of Acellular Nerve Scaffold and Application of PKH26 Fluorescent Labeling Combined with In Vivo Fluorescent Imaging System in Nerve Tissue Engineering. *Neurosci. Lett.* **2013**, *556*, 52−57.
(17) Swindle-Reilly, K.; Papke, J. B.; Kutosky, H. P.; Throm, A.; Hammer, J. A.; Harkins, A. B.; Willits, R. K. The Impact of Laminin on 3D Neurite Extension in Collagen Gels. *J. Neural. Eng.* **2012**, *9*, 046007.
(18) Mukhatyar, V. J.; Salmerón-Sánchez, M.; Rudra, S.; Mukhopadaya, S.; Barker, T. H.; García, A. J.; Bellamkonda, R. V. Role of Fibronectin in Topographical Guidance of Neurite Extension on Electrospun Fibers. *Biomaterials* **2011**, *32*, 3958−3968.
(19) Toba, T.; Nakamura, T.; Lynn, A. K.; Matsumoto, K.; Fukuda, S.; Yoshitani, M.; Hori, Y.; Shimizu, Y. Evaluation of Peripheral Nerve Regeneration Across an 80-mm Gap using a Polyglycolic Acid (PGA)−Collagen Nerve Conduit Filled with Laminin-Soaked Collagen Sponge in Dogs. *Int. J. Artif. Organs.* **2002**, *25*, 230−237.
(20) Yoshii, S.; Oka, M.; Shima, M.; Taniguchi, A.; Akagi, M. 30 mm Regeneration of Rat Sciatic Nerve Along Collagen Filaments. *Brain Res.* **2002**, *949*, 202−208.
(21) Cunha, C.; Panseri, S.; Antonini, S. Emerging Nanotechnology Approaches in Tissue Engineering for Peripheral Nerve Regeneration. *Nanomedicine* **2011**, *7*, 50−59.
(22) Gu, X.; Ding, F.; Williams, D. F. Neural Tissue Engineering Options for Peripheral Nerve Regeneration. *Biomaterials* **2014**, *35*, 6143−6156.
(23) Kehoe, S.; Zhang, X. F.; Boyd, D. FDA Approved Guidance Conduits and Wraps for Peripheral Nerve Injury: A Review of Materials and Efficacy. *Injury* **2012**, *43*, 553−572.
(24) Wang, Y.; Wei, Y. T.; Zu, Z. H.; Ju, R. K.; Guo, M. Y.; Wang, X. M.; Xu, Q. Y.; Cui, F. Z. Combination of Hyaluronic Acid Hydrogel Scaffold and PLGA Microspheres for Supporting Survival of Neural Stem Cells. *Pharm. Res.* **2011**, *28*, 1406−1414.
(25) Wen, X. J.; Tresco, P. A. Fabrication and Characterization of Permeable Degradable Poly (DL-Lactide-co-Glycolide) (PLGA) Hollow Fiber Phase Inversion Membranes for use as Nerve Tract Guidance Channels. *Biomaterials* **2006**, *27*, 3800−3809.
(26) Soldani, G.; Varelli, G.; Minnocci, A.; Dario, P. Manufacturing and Microscopical Characterisation of Polyurethane Nerve Guidance Channel Featuring a Highly Smooth Internal Surface. *Biomaterials* **1998**, *19*, 1919−1924.
(27) Wolfe, P. S.; Sell, S. A.; Bowlin, G. L. In *Tissue Engineering: From Lab to Clinic*; Pallua, N. S., Christoph, V., Eds.; Springer−Verlag: Heidelberg, Germany, 2011; p 41.
(28) Cheng, T.-Y.; Chen, M.-H.; Chang, W.-H.; Huang, M.-Y.; Wang, T.-W. Neural Stem Cells Encapsulated in a Functionalized Self-Assembling Peptide Hydrogel for Brain Tissue Engineering. *Biomaterials* **2013**, *34*, 2005−2016.
(29) Gelain, F.; Bottai, D.; Vescovi, A.; Zhang, S. G. Designer Self-Assembling Peptide Nanofiber Scaffolds for Adult Mouse Neural Stem Cell 3-Dimensional Cultures. *PLoS One* **2006**, *1*, 1−11.
(30) Sur, S.; Guler, M. O.; Webber, M. J.; Pashuck, E. T.; Ito, M.; Stupp, S. I.; Launey, T. Synergistic Regulation of Cerebellar Purkinje Neuron Development by Laminin Epitopes and Collagen on an Artificial Hybrid Matrix Construct. *Biomater. Sci.* **2014**, *2*, 903−914.
(31) Ghasemi-Mobarakeh, L.; Prabhakaran, M. P.; Morshed, M.; Nasr-Esfahani, M. H.; Ramakrishna, S. Bio-Functionalized Nanofibrous Scaffolds for Nerve Tissue Engineering. *Mater. Sci. Eng., C* **2010**, *30*, 1129−1136.
(32) Smith Callahan, L. A.; Xie, S.; Barker, I. A.; Zheng, J.; Reneker, D. H.; Dove, A. P.; Becker, M. L. Directed Differentiation and Neurite Extension of Mouse Embryonic Stem Cell on Aligned Poly(lactide) Nanofibers Functionalized with YIGSR Peptide. *Biomaterials* **2013**, *34*, 9089−9095.
(33) Banwell, E. F.; Abelardo, E. S.; Adams, D. J.; Birchall, M. A.; Corrigan, A.; Donald, A. M.; Kirkland, M.; Serpell, L. C.; Butler, M. F.; Woolfson, D. N. Rational Design and Application of Responsive Alpha-Helical Peptide Hydrogels. *Nat. Mater.* **2009**, *8*, 596−600.
(34) Mehrban, N.; Abelardo, E.; Wasmuth, A.; Hudson, K. L.; Mullen, L. M.; Thomson, A. R.; Birchall, M. A.; Woolfson, D. N. Assessing Cellular Response to Functionalized α-Helical Peptide Hydrogels. *Adv. Healthcare Mater.* **2014**, *3*, 1387−1391.
(35) Chelli, B.; Barbalinardo, M.; Valle, F.; Greco, P.; Bystrenova, E.; Bianchi, M.; Biscarini, F. Neural Cell Alignment by Patterning Gradients of the Extracellular Matrix Protein Laminin. *Interface Focus* **2013**, *4*, 20130041.
(36) Solozobova, V.; Wyvekens, N.; Pruszak, J. Lessons from the Embryonic Neural Stem Cell Niche for Neural Lineage Differentiation of Pluripotent Stem Cells. *Stem Cell Rev. Rep.* **2012**, *8*, 813−829.
(37) Greene, A. C.; Washburn, C. M.; Bachand, G. D.; James, C. D. Combined Chemical and Topographical Guidance Cues for Directing Cytoarchitectural Polarization in Primary Neurons. *Biomaterials* **2011**, *32*, 8860−8869.
(38) Palm, S. L.; Furcht, L. T. Production of Laminin and Fibronectin by Schwannoma Cells: Cell−Protein Interactions In Vitro and Protein Localization in Peripheral Nerve In Vivo. *J. Cell Biol.* **1983**, *96*, 1218−1226.
(39) Lefcort, F.; Venstrom, K.; McDonald, J. A.; Reichardt, L. F. Regulation of Expression of Fibronectin and its Receptor, $\alpha_5\beta_1$, during

DOI: 10.1021/acsbiomaterials.5b00051
ACS Biomater. Sci. Eng. 2015, 1, 431−439

Development and Regeneration of Peripheral Nerve. *Development* **1992**, *116*, 767−782.
(40) Tom, V. J.; Doller, C. M.; Malouf, A. T.; Silver, J. Astrocyte-Associated Fibronectin is Critical for Axonal Regeneration in Adult White Matter. *J. Neurosci.* **2004**, *24*, 9282−9290.
(41) Mathews, G. A.; ffrench-Constant, C. Embryonic Fibronectins are Up-Regulated Following Peripheral Nerve Injury in Rats. *J. Neurobiol.* **1995**, *26*, 171−188.
(42) Lefcort, F.; Clary, D. O.; Rusoff, A. C.; Reichardt, L. F. Inhibition of the NT-3 Receptor TrkC, Early in Chick Embryogenesis, Results in Severe Reductions in Multiple Neuronal Subpopulations in the Dorsal Root Ganglia. *J. Neurosci.* **1996**, *16*, 3704−3713.
(43) Vogelezang, M. G.; Scherer, S. S.; Fawcett, J. W.; ffrench-Constant, C. Regulation of Fibronectin Alternative Splicing during Peripheral Nerve Repair. *J. Neurosci. Res.* **1999**, *56*, 323−333.
(44) Johansson, S.; Svineng, G.; Wennerberg, K.; Armulik, A.; Lohikangas, L. Fibronectin-Integrin Interactions. *Front. Biosci.* **1997**, *2*, d126−d146.
(45) Noisa, P.; Urrutikoetxea-Uriguen, A.; Li, M.; Cui, W. Generation of Human Embryonic Stem Cell Reporter Lines Expressing GFP Specifically in Neural Progenitors. *Stem Cell Rev. Rep.* **2010**, *6*, 438−449.
(46) Mosmann, T. Rapid Colorimetric Assay for Cellular Growth and Survival: Application to Proliferation and Cytotoxicity Assays. *J. Immunol. Methods* **1983**, *65*, 55−63.
(47) Zhao, M.; Song, B.; Pu, J.; Wada, T.; Reid, B.; Tai, G.; Wang, F.; Guo, A.; Walczysko, P.; Gu, Y.; Sasaki, T.; Suzuki, A.; Forrester, J. V.; Bourne, H. R.; Devreotes, P. N.; McCaig, C. D.; Penninger, J. M. Electrical Signals Control Wound Healing Through Phosphatidylinositol-3-OH Kinase-γ and PTEN. *Nature* **2006**, *442*, 457−460.
(48) Wiese, C.; Rolletschek, A.; Kania, G.; Blyszczuk, P.; Tarasov, K. V.; Wersto, R. P.; Boheler, K. R.; Wobus, A. M. Nestin Expression- a Property of Multi-Lineage Progenitor Cells? *Cell. Mol. Life Sci.* **2004**, *61*, 2510−2522.
(49) Jacques, T. S.; Relvas, J. B.; Nishimura, S.; Pytela, R.; Edwards, G. M.; Streuli, C. H.; ffrench-Constant, C. Neural Precursor Cell Chain Migration and Division are Regulated Through Different β1 Integrins. *Development* **1998**, *125*, 3167−3177.
(50) Sheppard, A. M.; Brunstrom, J. E.; Thornton, T. N.; Gerfen, R. W.; Broekelmann, T. J.; McDonald, J. A.; Pearlman, A. L. Neuronal Production of Fibronectin in the Cerebral Cortex during Migration and Layer Formation is Unique to Specific Cortical Domains. *Dev. Biol.* **1995**, *172*, 504−518.
(51) Boekhoven, J.; Rubert Pérez, C. M.; Sur, S.; Worthy, A.; Stupp, S. I. Dynamic Display of Bioactivity through Host−Guest Chemistry. *Angew. Chem., Int. Ed.* **2013**, *52*, 12077−12080.
(52) Witze, E. S.; Connacher, M. K.; Houel, S.; Schwartz, M. P.; Morphew, M. K.; Reid, L.; Sacks, D. B.; Anseth, K. S.; Ahn, N. G. Wnt5a Directs Polarized Calcium Gradients by Recruiting Cortical Endoplasmic Reticulum to the Cell Trailing Edge. *Dev. Cell* **2013**, *26*, 645−657.
(53) Horwitz, A. R.; Parsons, J. T. Cell Migration- Movin' On. *Science* **1999**, *286*, 1102−1103.
(54) Webb, D. J.; Parsons, J. T.; Horwitz, A. F. Adhesion Assembly, Disassembly and Turnover in Migrating Cells- Over and Over and Over Again. *Nat. Cell Biol.* **2002**, *4*, E97−E100.
(55) Parsons, J. T.; Horwitz, A. R.; Schwartz, M. A. Cell Adhesion: Integrating Cytoskeletal Dynamics and Cellular Tension. *Nat. Rev. Mol. Cell Biol.* **2010**, *11*, 633−643.
(56) Burgess, B. T.; Myles, J. L.; Dickinson, R. B. Quantitative Analysis of Adhesion-Mediated Cell Migration in Three-Dimensional Gels of RGD-Grafted Collagen. *Ann. Biomed. Eng.* **2000**, *28*, 110−118.
(57) Winograd-Katz, S. E.; Fässler, R.; Geiger, B. Legate, K.R. The Integrin Adhesome: From Genes and Proteins to Human Disease. *Nat. Rev. Mol. Cell Biol.* **2014**, *15*, 273−288.
(58) Hynes, R. O. Integrins: Versatility, Modulation, and Signalling in Cell Adhesion. *Cell* **1992**, *69*, 11−25.
(59) Colognato, H.; Yurchenco, P. D. Form and Function: the Laminin Family of Heteromtrimers. *Dev. Dyn.* **2000**, *218*, 213−234.
(60) Aumailley, M.; Bruckner-Tuderman, L.; Carter, W. G.; Deutzmann, R.; Edgar, D.; Ekblom, P.; Engel, J.; Engvall, E.; Hohenester, E.; Jones, J. C.; Kleinman, H. K.; Marinkovich, M. P.; Martin, G. R.; Mayer, U.; Meneguzzi, G.; Miner, J. H.; Miyazaki, K.; Patarroyo, M.; Paulsson, M.; Quaranta, V.; Sanes, J. R.; Sasaki, T.; Sekiguchi, K.; Sorokin, L. M.; Talts, J. F.; Tryggvason, K.; Uitto, J.; Virtanen, I.; von der Mark, K.; Wewer, U. M.; Yamada, Y.; Yurchenco, P. D. A Simplified Laminin Nomenclature. *Matrix Biol.* **2005**, *24*, 326−332.
(61) Plantman, S.; Patarroyo, M.; Fried, K.; Domogatskaya, A.; Tryggvason, K.; Hammarberg, H.; Cullheim, S. Integrin-laminin Interactions Controlling Neurite Outgrowth from Adult DRG Neurons in vitro. *Mol. Cell. Neurosci.* **2008**, *39*, 50−62.
(62) Meng, X.-T.; Arocena, M.; Penninger, J.; Gage, F. H.; Zhao, M.; Song, B. P13K Mediated Electrotaxis of Embryonic and Adult Neural Progenitor Cells in the Presence of Growth Factors. *Exp. Neurol.* **2011**, *227*, 210−217.
(63) Tang, L.; Lu, Y.; Zheng, W.; Li, Y. Overexpression of MAP-2 via Formation of Microtubules Plays an Important Role in the Sprouting of Mossy Fibers in Epileptic Rats. *J. Mol. Neurosci.* **2014**, *53*, 103−108.
(64) Franze, K.; Guck, J. The Biophysics of Neuronal Growth. *Rep. Prog. Phys.* **2010**, *73*, 1−19.
(65) Crawford, A. H.; Stockley, J. H.; Tripathi, R. B.; Richardson, W. D.; Franklin, R. J. M. Oligodendrocyte Progenitors: Adult Stem Cells of the Central Nervous System? *Exp. Neurol.* **2014**, *260*, 50−55.
(66) Silver, J.; Miller, J. H. Regeneration Beyond the Glial Scar. *Nat. Rev. Neurosci.* **2004**, *5*, 146−156.
(67) Barth, L.; Sutterlin, R.; Nenniger, M.; Vogt, K. E. Functional Differentiation of Stem Cell-Derived Neurons from Different Murine Backgrounds. *Front. Cell. Neurosci.* **2014**, *8*, 49.
(68) Illes, S.; Fleischer, W.; Siebler, M.; Hartung, H. P.; Dihne, M. Development and Pharmacological Modulation of Embryonic Stem Cell-Derived Neuronal Network ctivity. *Exp. Neurol.* **2007**, *207*, 171−176.
(69) Wilcox, J. T.; Lai, J. K.; Semple, E.; Brisson, B. A.; Gartley, C.; Armstrong, J. N.; Bettes, D. H. Synaptically-Competent Neurons Derived from Canine Embryonic Stem Cells by Lineage Selection with EGF and Noggin. *PLoS One* **2011**, *6*, e19768.
(70) Addae, C.; Yi, X.; Gernapudi, R.; Cheng, H.; Musto, A.; Martinez-Ceballos, E. All-Trans-Retinoid Acid Induces the Differentiation of Encapsulated Mouse Embryonic Stem Cells into GABAergic Neurons. *Differentiation* **2012**, *83*, 233−241.
(71) Lai, H. C.; Jan, L. Y. The Distribution and Targeting of Neuronal Voltage-Gated Ion Channels. *Nat. Rev. Neurosci.* **2006**, *7*, 548−562.
(72) Song, M.; Mohamad, O.; Chen, D.; Yu, S. P. Coordinated Development of Voltage-Gated Na+ and K+ Currents Regulates Functional Maturation of Forebrain Neurons Derived from Human Induced Pluripotent Stem Cells. *Stem Cells Dev.* **2013**, *22*, 1551−1563.
(73) Johnson, M. A.; Weick, J. P.; Pearce, R. A.; Zhang, S. C. Functional Neural Development from Human Embryonic Stem Cells: Accelerated Synaptic Activity via Astrocyte Coculture. *J. Neurosci.* **2007**, *27*, 3069−3077.
(74) Guo, H. B.; Huang, L. Y.; Zou, Y. X.; Zou, F. Up-Regulation of the Transient A-type K+ Current (IA) in the Differentiation of Neural Stem Cells of the Early Postnatal Rat Hippocampus. *Chin. Med. J. (Engl.)* **2010**, *123*, 1731−1735.

DOI: 10.1021/acsbiomaterials.5b00051
ACS Biomater. Sci. Eng. 2015, 1, 431−439